LA-UR -78-1507

TITLE: Preprocessing of Seismic Signals for Pattern Recognition

AUTHOR(S): John E. Brolley

SUBMITTED TO: To be presented at the NATO Advanced Study Institute on Pattern Recognition and Signal Processing, June 25 - July 4, 1978, Paris, FRANCE.

MASTER

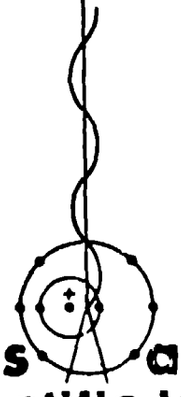

los alamos
scientific laboratory
of the University of California
LOS ALAMOS, NEW MEXICO 87545

Form No. 836
St. No. 2629
1/75

UNITED STATES
ENERGY RESEARCH AND
DEVELOPMENT ADMINISTRATION
CONTRACT W-7405-ENG. 36

Preprocessing of Seismic Signals for Pattern Recognition*

by

John E. Brolley
University of California
Los Alamos Scientific Laboratory
Los Alamos, New Mexico 87545, USA

ABSTRACT

This study describes the preparation of seismic signals in order to identify the best technique for input to a pattern recognition scheme. The signal is first filtered with zero phase shift high and low pass Butterworth filters. It is then subjected to adaptive filtering and finally moving average filtering. Spectral decomposition in terms of circular functions is done via conventional Fourier and log P maximum entropy analysis. Spectral decomposition in terms of sequency functions, Walsh, and Chebyshev, is also performed. The Walsh decomposition is done with the conventional fast operator. The Chebyshev decomposition is done with an optimization procedure. Results, based on these various operations, are presented for an underground nuclear explosion and several earthquakes.

INTRODUCTION

A vast corpus of seismic data is recorded daily, and presumably a significant portion of it is visually displayed for scrutiny by trained analysts. A goal of some analysts is to classify the source of the signal. In the present context two sources are considered; underground nuclear explosions and natural events. Essentially all of the events in the latter category will be earthquakes. In view of the impending Complete Test Ban (CTB), it is desirable to enhance the accuracy of the analyst's decision, and better still, to make a computer-generated decision. It may be possible to almost completely remove the human analyst from the decision process. This report is concerned with initial steps taken by the Digital Image and Signal Processing Group of the Los Alamos Scientific Laboratory towards the computer-based decision process.

*Work performed under the auspices of the U.S. Department of Energy, under Contract No. W7405-ENG-36.

Basically a characteristic feature of the seismogram is sought which tags the event unambiguously. In general, this may be a very difficult objective to achieve. However, it may be possible to supplement the seismogram tag with other information to minimize the error of decision.

Some obvious characteristics of a seismogram are time of arrival, duration, peak energy, total energy, and wave shape. The analysis to follow will be concerned mainly with the last two, and somewhat loosely with the others. All of the examples will be based on data recorded at the Albuquerque (ABQ) Seismic Research Observatory (SRO) of the United States Geological Survey (USGS). SRO stations are distributed around the world and represent the most modern facilities in the field.[1] The examples to be discussed will utilize the short period data, 20 samples per second, and consideration of the short period gain curve will be given.

DATA

Three sequences of short period data will be considered. In the plots to be presented the horizontal axis is time and the vertical axis is a measure of ground motion at ABQ. The calibration of an SRO is such that 2×10^6 digital counts equals 1 micron of ground displacement at 1 s period. All three sets include 20 s of data prior to the onset of the signal.

The seismogram of an underground nuclear explosion at the Nevada Test Site (NTS) is displayed in Fig. 1. The first 2048 points are plotted. The second seismogram was produced by an earthquake in Utah. The coordinates were lat. 40.51 N, long. 110.28 W. The origin time was 30 September 1977, 10:19:19.6 GMT. This was a normal earthquake with the nodal plane of the focal mechanism solution for the near shock striking NNW and dipping to the NE. The epicenters were confined to an area 5 x 2 km. The hypocenters were in the depth range 2-8 km with most activity in the range 4-8 km. The magnitude was M_L = 5.1 (National

Earthquake Information Service, Golden, Colorado). Aftershocks continued for several weeks; one aftershock on 11 October 1977, 0756 GMT, reached a magnitude of M_L = 4.7. The Utah seismogram will be referred to as UTAH. The first 2048 points are displayed in Fig. 2.

The second earthquake occurred near the California-Mexico border. Its coordinates were lat. 32.47°N, long. 115.18 W, and the origin time was 17 January 1977, 11:13:19.4 GMT. This earthquake has not been subjected to detailed analysis yet. Preliminary indications are that its magnitude was M_L = 4.2, with a depth of 5 km. It will be referred to as CALMEX. The first 2048 points of its seismogram are displayed in Fig. 3.

UTAH had the longest duration signal at ABQ/SRO. It lasted approximately four times longer than the other two.

The approximate positions of the three sources with respect to ABQSRO are shown in Fig. 4.

The three seismograms will now be used to illustrate various aspects of signal processing.

FILTERING

The simplest form of filtering is leveling in the amplitude domain. All three data sequences were scanned and the amplitudes proportionately reduced so that the maximum amplitude in any sequence was unity. This can also be viewed as a form of normalization. When all subsequent filtering operations have been performed, the total energy in the signal is computed. All amplitudes are then divided by the square root of the total energy. This is called total energy normalization.[2] It is not implied that this is the optimum normalization technique. The three sequences contain energy of frequencies that one may not wish to consider during a particular mode of analysis. Moreover, frequencies outside the band of interest may complicate the interpretation of frequencies

of interest.[3] For these reasons high- and low-pass, three section Butterworth digital filters with zero phase shift have been constructed. These filters have smooth top and bottom roll-off with no ripple.[3] Bandpass filtering is available by operating the high- and low-pass filters in tandem. The result of bandpass filtering the NEVADA data is shown in Fig. 5. In this case the cutoff of the high-pass filter was 0.5 Hz, and the low pass, 5.0 Hz. It will be noted that the wide ranging excursions apparent in the first 20 s before onset have been removed.

It is possible that signals may come through the passband that has been used, which are not related to the seismic signal and may contribute some uncertainty in the analysis. In some cases this undesirable effect can be reduced. It is possible to construct a digital filter that is smart. If such a filter has the opportunity to observe, as it were, a signal, and if the signal is reasonably stationary, the filter can memorize the pattern and reject it. This is called adaptive filtering.[4,5] The adaptive filters used in this work are nonrecursive. Recursive types will be studied shortly. Both types are suitable for real-time operation. The amount of training data in the three sequences is only 20 s long. This can be extended in future work. The 20 s period may not be long enough for the filter to generate as much reduction as possible, i.e., the training period may be too short. At the onset of the desired signal the filter configuration is frozen. The application of a 20 element filter, whose adaptive rate[5] was 0.04, to NEVADA is shown in Fig. 6. It is clear by comparison with Fig. 1 that in the short training interval the filter is learning to remove some low frequency components.* In-depth studies of this type of filtering are planned. The result of operating on NEVADA with all the filters discussed so far is shown in Fig. 7.

Moving average filters is sometimes used advantageously after adaptive filtering.[5] The result of operating on the sequence shown in Fig. 7 with a

*See Appendix A for an additional example.

moving average filter of length 5 is shown in Fig. 8. In what follows, CALMEX and UTAH were processed in precisely the same manner as NEVADA.

WAVE SHAPE

The description of a time series or wave in terms of an expansion utilizing circular functions has a hoary tradition and is ardently practiced by most students of the seismogram. However, for a given number of terms, it does not provide the most faithful description. The Karhuenen-Loeve (KL) (sometimes called KARLOV) achieves the best fit.[6] This achievement comes at the expense of great computing labor.

However, it has been conjectured that the most accurate representation may not provide the best differentiating capability.[7] It appears that there is an analytical basis for this conjecture.[6] In the present discussion, a pragmatic approach will be indicated, although a semi-rigorous investigation may be made later.

It will be assumed that the seismic signal can be built up by assembling various types of building blocks. For the present three types of blocks will be considered; circular functions, Walsh functions, and Chebyshev functions. Others could be added to the list. There are various ways of stacking these blocks to build seismic signals. Three that will be considered here are the fast projection operator, e.g., Fast Fourier Transform (FFT), log P maximum entropy, and optimization theory. Other approaches exist[8] and may be applied. In the following examples the appropriate operator acted on 64 consecutive data points and generated a power spectrum. Successive spectra were produced by displacing the operator 16 points in the direction of increasing time.

In the case of circular functions, two types of operators were employed. The first was the conventional FFT with a Hamming window encompassing the 64 data points. Thus, a three-dimensional plot of Fourier power can be generated. In what will follow, these surfaces have been smoothed somewhat with

two-dimensional twice Tukey filtering. A prescription for this is sketched in Appendix B. For the present only power in the higher frequencies will be indicated. In order to more clearly visualize this distribution, power corresponding to Fourier function indices 1 to 6 have been set to zero. In addition, two-dimensional twice Tukey filtering, as done here, removes four border points all the way around the plot, a matter of no consequence for the present discussion. In Fig. 9 the Fourier power surface for the first 2048 points of NEVADA is displayed. The right hand corner is the origin of time and frequency. Time flows upward, and frequency flows to the left. The frequency index at which power is first plotted is 7. In the usual ordering, the index 1 corresponds to DC, 2 to one cycle, etc. Since each sequence is 64 points (63 x .05 = 3.15 sec) the first plotted frequency is 6/3.15=1.9 Hz, and the highest frequency shown on the plot is 4.44 Hz. The use of synthetic signals in the code is useful for checking performance. Thus, a damped sine wave starting at point 100 and running out to 2048 points is Fourier analyzed and is shown in Fig. 10. The damped sine had a frequency of 3.492 Hz, and therefore, should correspond to a function index of 12. The two-dimensional twice Tukey filter has removed the first 4 indices and the peak of the power occurs at 8 on the plot as it should. A wide range of synthetic signals is available in the code for studying various modes of analysis.

Burg's log P maximum entropy analysis was applied next to NEVADA. There appears in this operator a filter length parameter which will require some study. Richer[9] has given a prescription for evaluating it but there does not seem to be unanimity of views on this point.[10] With a filter length of 20 the result shown in Fig. 11 was obtained from NEVADA. The maximum entropy operator was not windowed.

There are many noncircular functions available for building blocks, and two examples will be considered here. Walsh functions constitute a complete

orthonormal set having amplitudes +1, -1, and are, therefore, computationally relatively simple to deal with. A comparison of the first few Walsh functions with circular functions is given in Fig. 12. Corresponding to the concept of frequency as applied to circular functions, there exists the analogous concept of sequency for Walsh functions. In this case, sequency is defined as one-half the number of zero crossings over the time base. The first zero crossing at the beginning of the time base is not counted. Analogous to the FFT operator, there exists a fast operator for Walsh functions, FWT. This has been applied in manner similar to the Fourier case except that the data window was a triangle. The result of acting on the NEVADA data with the Walsh operator is shown in Fig. 13. Walsh analysis indicates more high-sequency power than Fourier analysis,[7] a feature which may be useful in the pattern recognition problem.

Another set of building blocks is the orthonormal set of Chebyshev polynomials defined over the range of argument - 1 to + 1. A plot of the first five is shown in Fig. 14. The concept of sequency may also be used here. For this discussion Chebyshev sequency will be defined as the number of zero crossings over the argument range -1 to +1. Perhaps it should be called Chebquency. The operator used here for evaluating Chebyshev sequency power differs from the fast operators previously alluded to. Basically, it performs an optimized fit of a given set of polynomials to a sequence of arbitrary length. For purposes of comparison with the other methods, 32 polynomials are used over a time base of 64 points. No windowing has been done. The result of acting on NEVADA with the Chebyshev operator is shown in Fig. 15. This plot and those that follow differ from the previous set in that only the DC term has been equated to zero. Also the vertical scaling factor is no longer automatic, but is fixed at a particular value. As in the other examples the sharp rise of high-sequency power occurs at the beginning of the seismic signal and then dies out.

It is interesting to compare this plot with the earthquake CALMEX (Fig. 2). Identical operations on the earthquake signal produced the result shown in Fig. 16. The plotting can be done quantitatively by passing planes through the peaks of power, i.e., contour plotting. The corresponding contour plot of NEVADA for three levels of power is shown in Fig. 17, and for CALMEX in Fig. 18. The same contour plot for UTAH (Fig. 3) is shown in Fig. 19.

CONCLUSIONS

Adaptive filtering, zero phase shift Butterworth filtering, moving average, and twice Tukey filtering have been incorporated in a seismic signal analysis code. Four modes of spectral decomposition are available for study: Fourier, Walsh, log P maximum entropy, and Chebyshev. Different power signatures have been noted for this set which may be augmented. A set of training data is on hand. A study can then be made to ascertain which combination of spectral decomposition and pattern recognition provides the best differentiating capability between seismic signals from natural events and underground nuclear explosions.

ACKNOWLEDGMENTS

I acknowledge, with pleasure, the vital and generous help received from four branches of the USGS. J. Peterson and J. Hoffman of ABQ/SRO have spent much time explaining SRO and providing all the data used in this paper. C. Langer of the Denver office provided the information on UTAH. G. Fuis of the Pasadena office provided information on CALMEX. J. F. Evernden, National Earthquake Research Center, has patiently explained some of the intricacies of geophysics and spectral problems.

N. Ahmed of Kansas State University, G. Elliot, S. Sterns, and W. Jacklin of Sandia Laboratory have given valuable guidance in various aspects of signal processing.

At Los Alamos, G. Wecksung guided the two-dimensional twice Tukey filtering, and J. House, R. Saunders, and N. Ginther helped in data acquisition. M. Cannon and R. Frank translated data tapes to local system files.

This work was made possible by the support and encouragement of W. E. Deal and D. H. Janney.

APPENDIX A

Example of Adaptive Filtering

The synthetic signal feature of the seismic code can be used to illustrate rather clearly the action of the adaptive filter. Figure 20 displays a synthetic composite data sequence 2048 points long. One sine wave of amplitude 1, frequency 3.48 Hz, starts at point 100 and runs without damping. A second sine wave starts at point 1000 with amplitude 0.1 and frequency 3.0 Hz, and is strongly damped. The filter was instructed to stop learning at point 995, and freeze its configuration after that. Its adaptive rate was 0.01. The results are shown in Fig. 21. Some appreciation of the signal to noise gain can be seen in the blown up plot of Fig. 22.

APPENDIX B

A Prescription for Two-Dimensional Twice Tukey Filtering

Given an n x m Matrix X.

Form a 5-point sampling cross

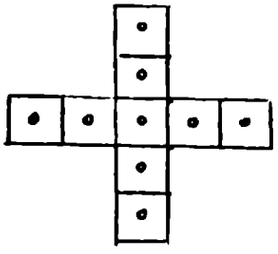

to operate on X. This operator starts for convenience in the upper left-hand corner of X such that the uppermost of the five vertical point samples the values in row one and the left-most in the horizontal set of five samples, the points in the first column. Nine values are obtained. The median value is extracted and loaded in the new matrix Y at $Y_{1,1}$. The operator is then stepped across X column by column until the right-most cell of the cross samples the last column, thereby filling up the first row of Y. The operator is displaced one row down and the operation repeated, etc. Y will then be (n-4)x(m-4). Form X-Y with Y placed symmetrically in X and the overlap thrown away. Repeat the cross operation on X-Y to form S. The final result is Y+S where overlap has been discarded. S is now (n-8)x(m-8). The reader may wish to consult Ref. 11.

REFERENCES

1. J. Peterson, H. M. Butler, L. G. Holcomb, and G. R. Hutt, "The Seismic Research Observatory," Bull. Seism. Soc. Amer. 66, 2049 (1976).

2. W. R. Youngblood, "Seismic Discrimination by Harmonic Analysis Techniques," AFIT-EN GE/EE/72-29.

3. S. D. Stearns, Digital Signal Analysis, Hayden, Rochelle Park, NJ, 1975.

4. G. R. Elliott, "Improving the Performance of Perimeter Security Sensors Through Digital Signal Processing," Proc. Digital Signal Processing Symposium, Sandia Lab, Albuquerque, NM, SAND 77-1845C, 1977.

5. N. Ahmed, "On Intrusion-Detection via Adaptive Filtering," SAND 77-1845C, 1977.

6. T. Pavlidis, Structural Pattern Recognition, Springer-Verlag, Berlin, 1977.

7. J. E. Brolley, "Preliminary Code Development for Seismic Signal Analysis Related to Test Ban Treaty Questions," SAND 77-1845C, 1977.

8. J. E. Brolley, R. B. Lazarus, B. R. Suydam, and H. J. Trussell, "Maximum Entropy Analysis for Some One- and Two-Dimensional Problems," SAND 77-1845C, 1977.

9. H. B. Richer and T. J. Ulrych, "High Frequency Optical Variables," Ap. J. 192, 719 (1974).

10. H. B. Radoski, P. F. Fougere, and E. J. Zowalick, "A Comparison of Power Spectral Estimates and Applications of Maximum Entropy Method," J. Geophys. Resch., 80, 619 (1975).

11. R. W. Hamming, Digital Filters, Prentice-Hall, Englewood Cliffs, NJ, 1977.

CAPTIONS

Fig. 1. First 2048 points of NEVADA data from ABQ/SRO.

Fig. 2. First 2048 points of UTAH data from ABQ/SRO.

Fig. 3. First 2048 points of CALMEX data from ABQ/SRO.

Fig. 4. Geographical disposition of sources and detector.

Fig. 5. Bandpass filtered NEVADA data.

Fig. 6. Adaptive filtering of NEVADA data.

Fig. 7. Bandpass plus adaptive filtering of NEVADA data.

Fig. 8. Bandpass plus adaptive plus moving average filtering of NEVADA data.

Fig. 9. Fourier power spectrum of NEVADA.

Fig. 10. Fourier power spectrum of a damped sine wave.

Fig. 11. Log P maximum entropy power spectrum of NEVADA.

Fig. 12. Comparison of some Walsh and circular functions.

Fig. 13. Walsh power spectrum of NEVADA.

Fig. 14. First 5 Chebyshev polynomials.

Fig. 15. Three-dimensional Chebyshev power spectrum of NEVADA.

Fig. 16. Three-dimensional Chebyshev power spectrum of CALMEX.

Fig. 17. Three-level contour plot of Chebyshev power spectrum of NEVADA.

Fig. 18. Three-level contour plot of Chebyshev power spectrum of CALMEX.

Fig. 19. Three-level contour plot of Chebyshev power spectrum of UTAH.

Fig. 20. Synthetic data: continuous sinewave plus damped sinewave.

Fig. 21. Adaptive filter output for the input shown in Fig. 20.

Fig. 22. Expanded view of the filter output around the damped wave.

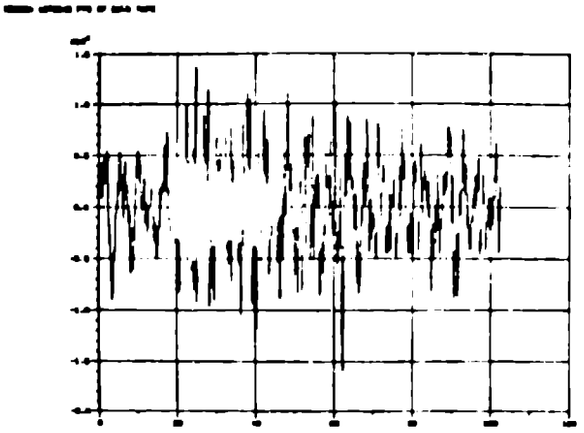

Fig. 1. First 2048 points of NEVADA data from ABQ/SRO.

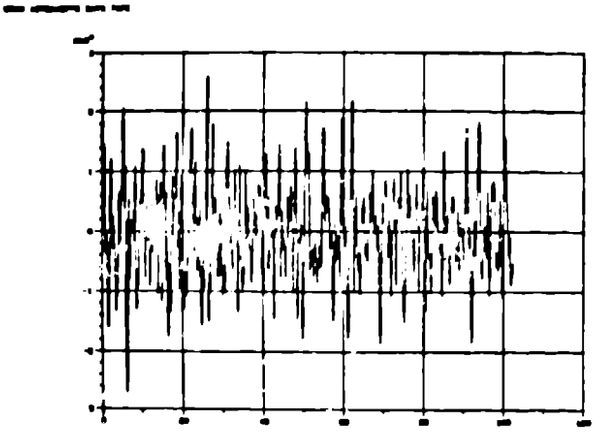

Fig. 2. First 2048 points of UTAH data from ABQ/SRO.

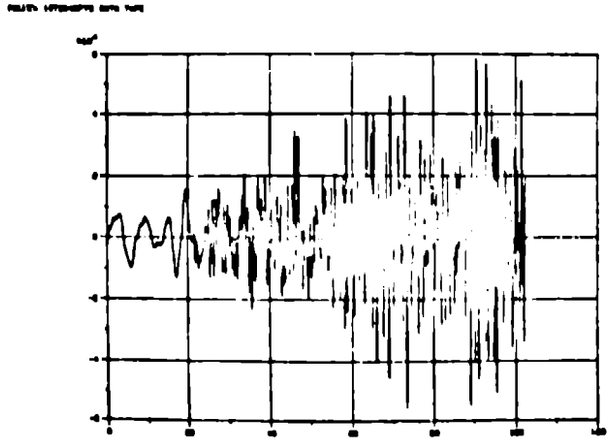

Fig. 3. First 2048 points of CALMEX data from ABQ/SRO.

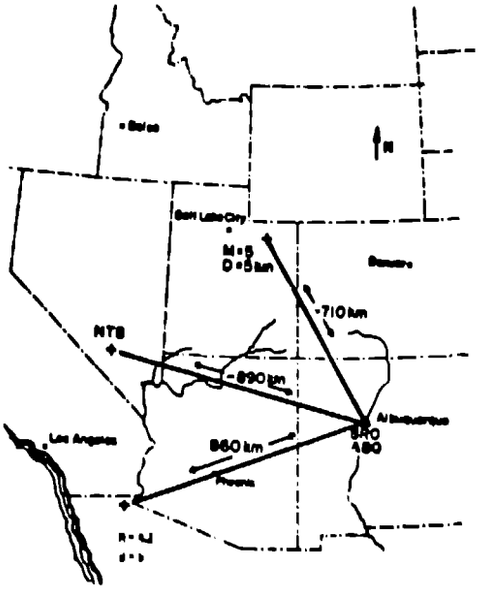

Fig. 4. Geographical disposition of sources and detector.

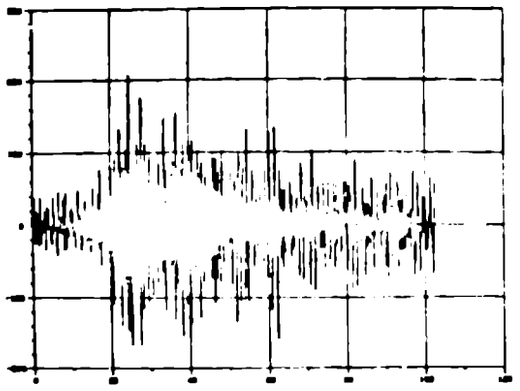

Fig. 5. Bandpass filtered NEVADA data.

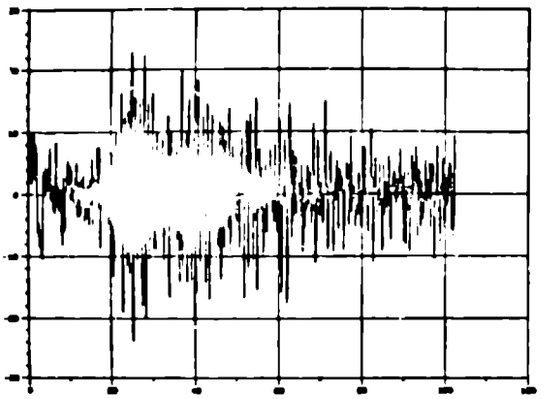

Fig. 6. Adaptive filtering of NEVADA data.

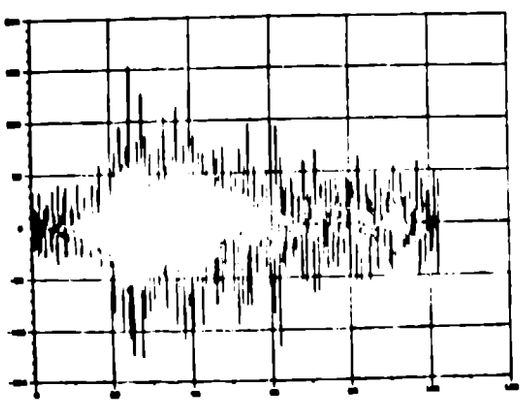

Fig. 7. Bandpass plus adaptive filtering of NEVADA data.

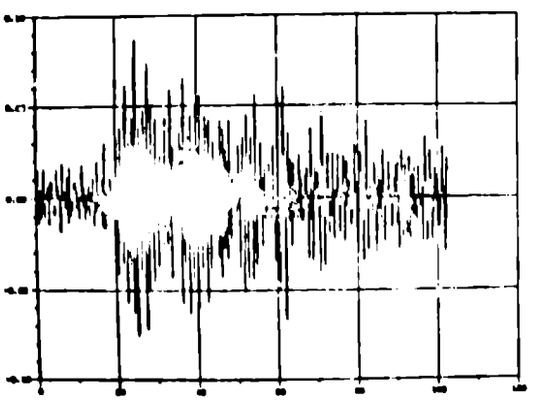

Fig. 8. Bandpass plus adaptive plus moving average filtering of NEVADA data.

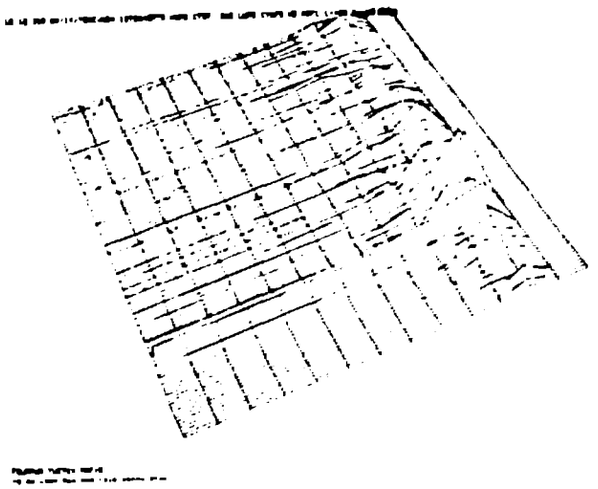

Fig. 9. Fourier power spectrum of NEVADA.

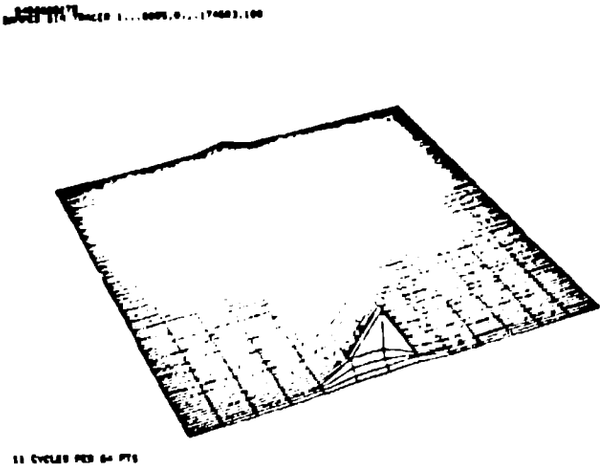

Fig. 10. Fourier power spectrum of a damped sine wave.

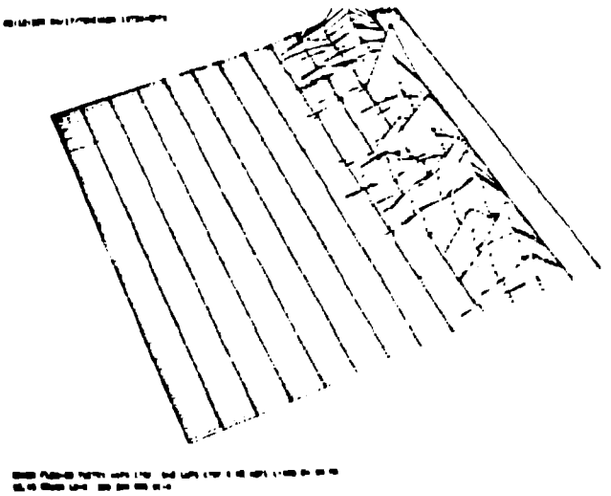

Fig. 11. Log P maximum entropy power spectrum of NEVADA.

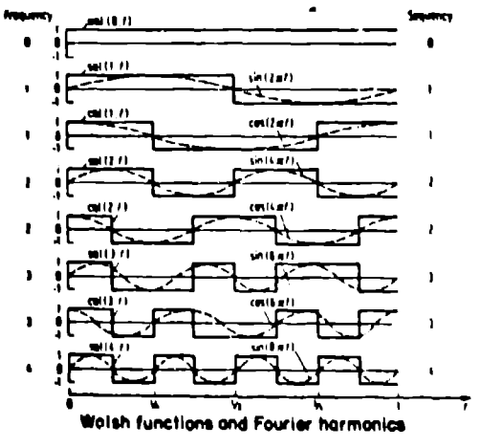

Fig. 12. Comparison of some Walsh and circular functions.

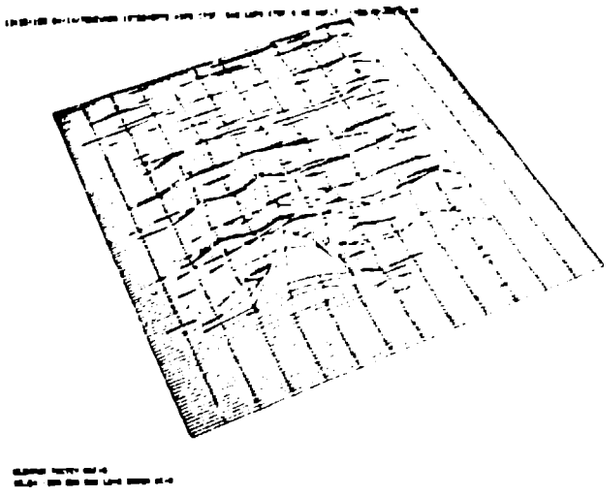

Fig. 13. Walsh power spectrum of NEVADA.

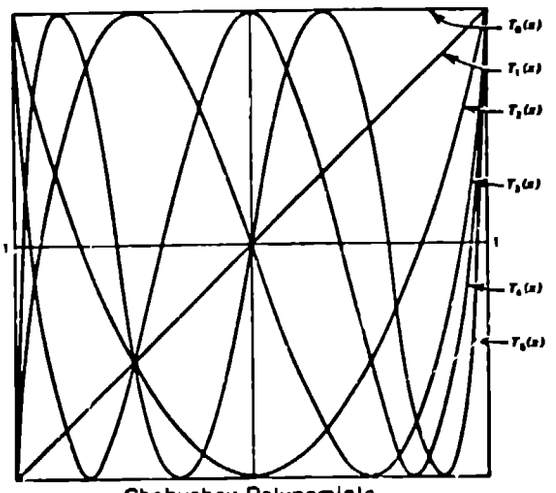

Fig. 14. First 5 Chebyshev polynomials.

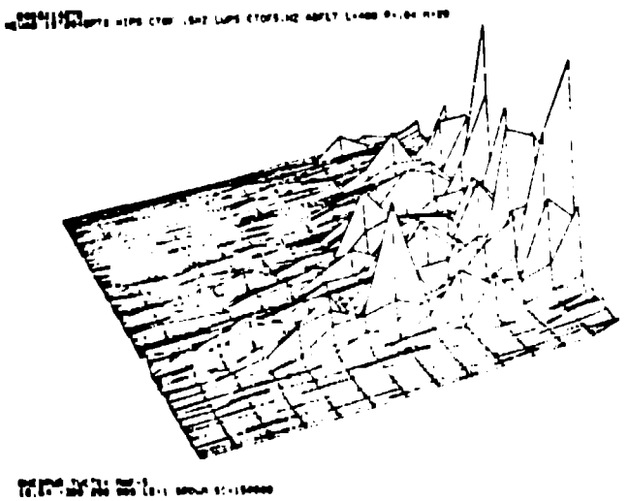

Fig. 15. Three-dimensional Chebyshev power spectrum of NEVADA.

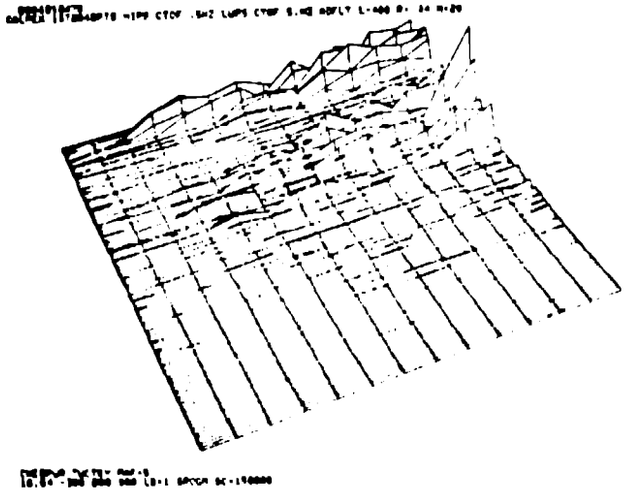

Fig. 16. Three-dimensional Chebyshev power spectrum of CALMEX.

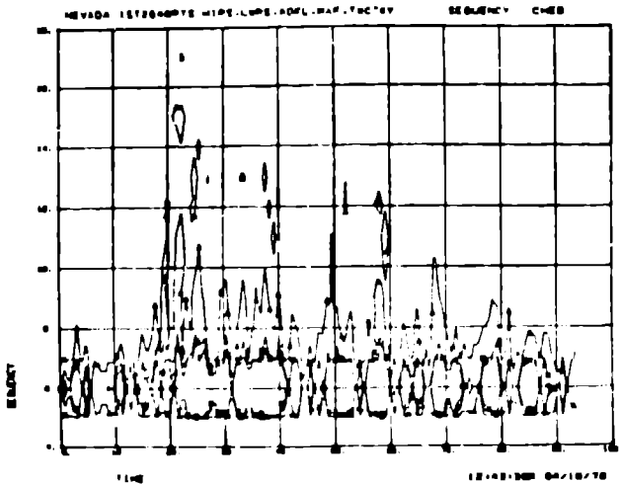

Fig. 17. Three-level contour plot of Chebyshev power spectrum of NEVADA.

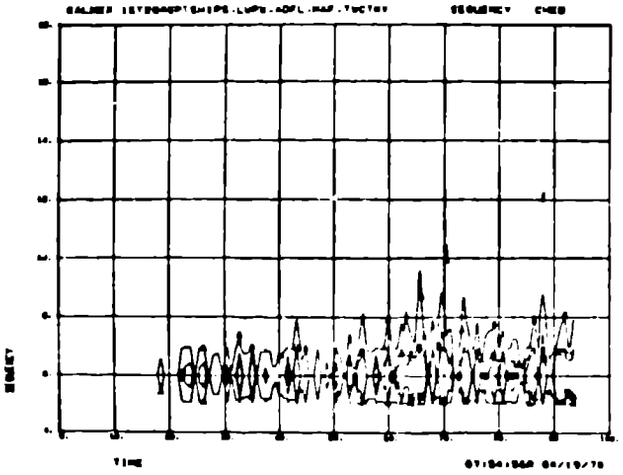

Fig. 18. Three-level contour plot of Chebyshev power spectrum of CALMEX.

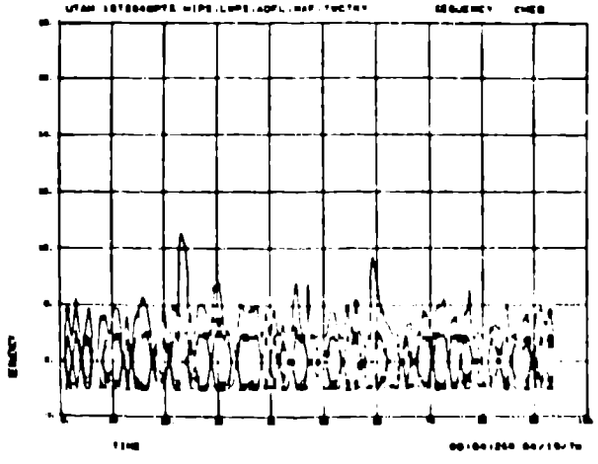

Fig. 19. Three-level contour plot of Chebyshev power spectrum of UTAH.

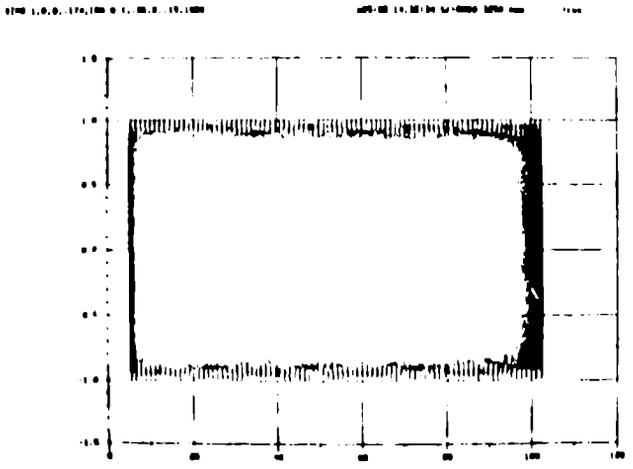

Fig. 20. Synthetic data: continuous sinewave plus damped sinewave.

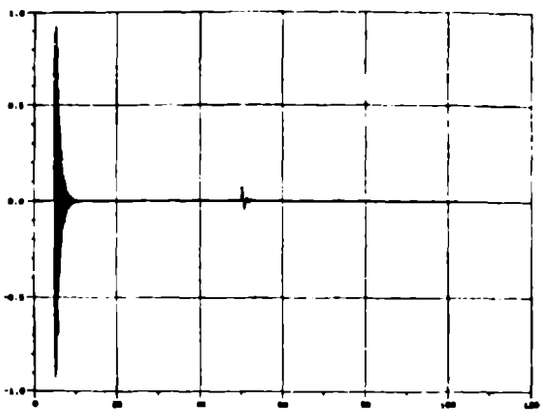

Fig. 21. Adaptive filter output for the input shown in Fig. 20.

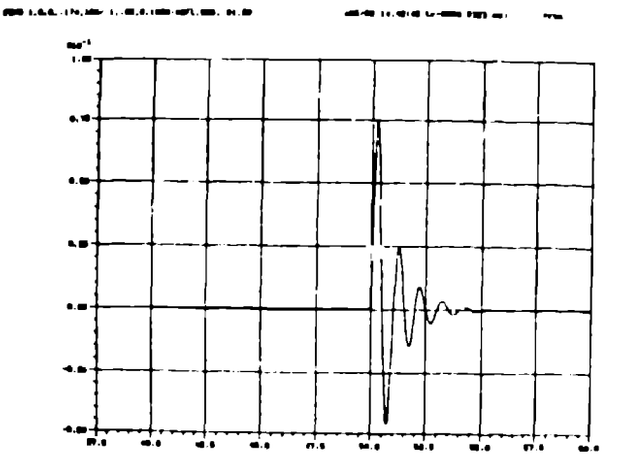

Fig. 22. Expanded view of the filter output around the damped wave.